Astron. Astrophys. 338, 1102–1108 (1998)

ASTRONOMY AND ASTROPHYSICS

The solar transition region: a time-varying interface between the chromosphere and corona?

E. O'Shea[1], **J.G. Doyle**[2], **and F.P. Keenan**[1]

[1] Department of Pure & Applied Physics, The Queen's University of Belfast, Belfast BT7 1NN, N.Ireland, UK (E.Oshea@queens-belfast.ac.uk; F.Keenan@queens-belfast.ac.uk)
[2] Armagh Observatory, College Hill, Armagh BT61 9DG, N. Ireland, UK (jgd@star.arm.ac.uk)

Received 20 May 1998 / Accepted 5 August 1998

Abstract. Using joint observations taken with the CDS and SUMER instruments onboard SOHO, we re-examine the solar transition region in an attempt to determine whether it is de-coupled from the over-lying coronal region. Line ratios calculated from temporal series observations of O IV and Fe XIII spectral lines were converted to electron density, and hence electron pressure using theoretical line ratios. Little or no evidence was found to support the constant electron density assumption, and instead a constant electron pressure is found between the transition region and corona. This lends support to the idea that the transition region is a time varying interface between the chromosphere and corona, and is not formed in unresolved fine-structures that are disconnected from the corona.

Key words: atomic data – Sun: transition region – Sun: corona – Sun: UV radiation

1. Introduction

The SOHO mission, launched in December 1995, contains an array of instruments for studying the solar atmosphere. Of these, only the Coronal Diagnostic Spectrometer (CDS) (Harrison et al. 1995) and Solar Ultraviolet Measurement of Emitted Radiation (SUMER) (Wilhelm et al. 1995, 1997) are suitable for observing a range of spectral lines, and hence the derivation of electron densities. Using joint observations obtained from these two instruments, we have determined the electron density in the transition region and corona, in order to evaluate whether the solar transition region is magnetically and thermally decoupled from the over-lying corona. Before describing the observations in Sect. 3, we will briefly review the background to this work.

It has been found that even with very good atomic physics data it is not always possible to get consistent results between theoretical and observed intensity ratios. For example emission lines from Be and Mg-like ions, such as Ca XVII and Fe XV, show anomalous results. It has been suggested that the reason for this difference is due to the fact that the plasma is not in equilibrium but is subject to compression by frequent small explosive events or bursts (Laming & Feldman 1992, Feldman et al. 1992, Feldman & Laming 1993). The suggestion is that the plasma is compressed on time-scales which do not allow equilibrium conditions to prevail. This idea was first developed as a way of explaining why the emission lines of neutral and singly ionized helium have larger intensities than would be expected from calculations. Laming & Feldman (1992) noted that this situation would be observed if the temperature of the line excitation was raised while the ionization balance was kept close to that of a lower quiescent temperature. They proposed that the chromosphere is heated by frequent small explosive events or bursts, rising the temperature of small regions of the plasma in time-scales short compared to the ionization equilibrium time.

Similarly, Feldman (1992) proposed that the discrepancy in the electron density determination obtained from Fe IX line ratios, when compared to other line ratios, could also be explained by a burst model. Fe IX ions whose lifetimes in the burst were shorter than the lifetime of the excited level from which the diagnostic radiation is emitted should have that particular line intensity reduced. It has been further proposed that if the transition region is continuously heated by these small bursts, then the notion that this region obeys a constant electron pressure law with the higher temperature atmosphere is incorrect, and that a constant electron density more closely fits the observations (Feldman & Laming 1993). Here, we use data obtained in July 1996 in a joint CDS/SUMER observational campaign to test the constant electron density hypothesis.

2. Atomic data and theoretical ratios

2.1. Fe XIII

The diagnostic potential of Fe XIII emission lines, due to $3s^2 3p^2$-$3s3p^3$ transitions, was first noted by Flower & Pineau des Forets (1973) and Flower & Nussbaumer (1974). The latter presented possible electron density sensitive emission line ratios calculated using electron excitation rates generated in the Distorted Wave approximation. Subsequently this ion has been used successfully for a density diagnostic of active regions and flares (see for example, Dere et al. 1979, Dere 1982). More recently Keenan et al. (1995) used Fe XIII emission lines to infer electron densities for solar active regions and for two stars, α Cen and Procyon.

Send offprint requests to: E. O'Shea

Table 1. A log of the various density datasets observed with the CDS and SUMER instruments.

Date	Instrument	Dataset	Pointing X,Y	Start UT	End UT	Lines observed (Å)
9 July '96	CDS	s3477r01	$+537, -205$	15:49	16:35	Fe XIII 359/348
	CDS	s3479r00	$+537, -205$	18:08	18:53	Fe XIII 359/348
	SUMER	sum_960709_165749	$+531, -200$	16:57	17:31	O IV 1407/1401
	SUMER	sum_960709_173109	$+531, -200$	17:31	18:04	O IV 1407/1401

The model ion for Fe XIII, used by Keenan et al. (1995), consisted of the eight energetically lowest LS states $3s^2 3p^2\ ^3P_{0,1,2}$,$^1D_2$ and $^1S_0$; $3s3p^3\ ^3D_{1,2,3}$, $^3P_{0,1,2}$, $^1D_2$, $^3S_1$ and $^1P_1$, making a total of 14 fine-structure levels. Using the model ion above together with the statistical equilibrium code of Dufton (1977) relative Fe XIII level populations and hence emission-line strengths were calculated as a function of electron density at the temperature of maximum fractional abundance of Fe XIII, Log T_e=6.2 K(Arnaud & Rothenflug, 1985).

By using the same theoretical data as Keenan et al. (1995) we will examine the ratio;

R_1 = I($3s^2 3p^2\ ^3P_1$ - $3s3p^3\ ^3D_{1,2}$)/I($3s^2 3p^2\ ^3P_0$ - $3s3p^3\ ^3D_1$)
= I(359.64Å)/I(348.18Å).

2.2. O IV

Ions in the boron isoelectronic sequence are frequently used for diagnostic purposes, as first outlined by Flower & Nussbaumer (1975). Subsequent papers based on B-like ions include Vernazza & Mason (1978), Doschek (1984), and Dwivedi & Gupta (1992, 1994).

The ratio we will examine in this work is;

R_2= I(1407.39Å)/I(1401.16Å).

Both these lines belong to the transition $2s^2 2p\ ^2P^o \rightarrow 2s2p^2\ ^4P$ which produces lines at 1407.4, 1404.8, 1401.1, 1399.7 and 1397.2Å.

The atomic data adopted in the calculation of the O IV I(1407.39Å)/I(1401.16Å) intensity ratio are as discussed in the paper by O'Shea et al. (1996) with the exception of the Einstein A-coefficients for the $2s^2 2p\ ^2$P–$2s2p^2\ ^4$P inter-combination lines. These are the transitions that produce the range of O IV lines between 1397 and 1407Å. Brage et al. (1996) have recently recalculated radiative rates for these transitions, and shown that the data of Nussbaumer & Storey (1982) employed by O'Shea et al. are in error. The results of Brage et al. were therefore used in the line ratio calculations, although it should be noted that these lead to theoretical values for most line ratios within a few percent of those of O'Shea et al. and Cook et al. (1995). This is not the case for line ratios involving the O IV 1404.81Å transition, where the Brage et al. diagnostics are up to $\simeq$20% different. However we do not employ the 1404.81Å line as a diagnostic, as it is blended with a S IV transition at 1404.77Å (Cook et al. 1995).

The model ion used for calculating the theoretical line ratios of O IV consisted of the 15 energetically lowest fine-structure levels, namely $2s^2 2p\ ^2P_{1/2,3/2}$; $2s2p^2\ ^4P_{1/2,3/2,5/2}$, $^2D_{3/2,5/2}$, $^2S_{1/2}$, $^2P_{1/2,3/2}$; $2p^3\ ^4S_{3/2}$, $^2D_{3/2,5/2}$ and $^2P_{1/2,3/2}$.

As the theoretical data for O IV and Fe XIII used in this work came from the Keenan et al. group working in Queen's University Belfast (QUB), results from these data will be referred to subsequently as the QUB results.

2.3. CHIANTI

The second source of theoretical line ratios used in this work come from the CHIANTI database. CHIANTI consists of a collection of critically evaluated data necessary to calculate the emission line spectrum of an astrophysical plasma (Dere et al., 1997). It consists of a database of atomic energy levels, electron collisional excitation rates and atomic radiative data such as oscillator strengths and A-values. A set of programs written in IDL (Interactive Data Language) uses these data to solve the statistical equilibrium equations providing theoretical line intensity ratios, synthetic spectra and the differential emission measure. The collisional data comes from a number of sources which employed both R-matrix and distorted wave calculations. In general, the excitation rates used by both O'Shea et al. (1996) and Keenan et al. (1995) are similar to those used by the CHIANTI project. For example the O IV atom of both groups used the R-matrix excitation rates from Zhang et al. (1994). However for Fe XIII, CHIANTI used excitation rates calculated using the Distorted Wave approximation while Keenan et al. (1995) used the excitation rates from Tayal (1995) which were calculated using the R-matrix method. Energies are typically taken from databases of observed energy levels (see Dere et al. 1997 for details) and supplemented by the best theoretical estimates available. CHIANTI does not include proton excitation rates which may be important for fine structure transitions in highly ionised systems. As shown above these were included for the O IV atomic data used by O'Shea et al. (1996). For the O IV model atom the 125 lowest energy levels were used, while for Fe XIII the lowest 27 levels were used.

3. Observational data

3.1. CDS observations

The observations were taken of an active region at coordinates X$\simeq$530, Y$\simeq$–200 on the 9th July 1996. In Table 1 a summary of the different observations carried out by the two instruments is given. The relative starting position of the slit for each dataset may be seen in Fig. 1 and are discussed further in Sect. 4.1.

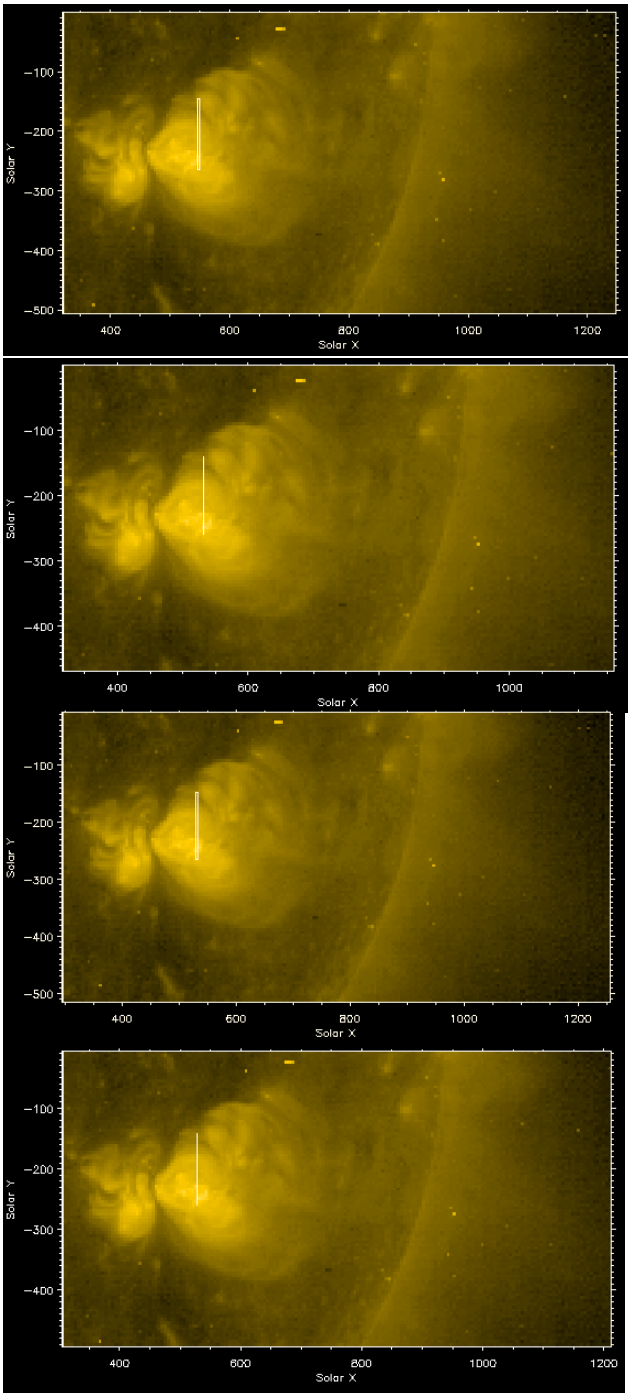

Fig. 1. An image of the Sun taken with EIT (courtesy of the EIT consortium) showing the position of the slit for datasets s3477r01 (top row), 165749 (second row), s3477r01 (third row) and 173109 (bottom row) on the 9th July 1996. This EIT image was taken in Fe XV 284Å at 17:09 UT. The axes are in units of arc sec from disk centre. Note the position of the limb at ∼800-900 arc sec.

The CDS observations were taken using the 308–381Å region of the Normal Incidence Spectrometer (NIS). Within this wavelength range there are two potentially useful electron density sensitive line ratios involving lines of Fe XIII. These are Fe XIII 359.64/348.18 and Fe XIII 318.12/320.80. Despite there being a small amount of blending of the Fe XIII 359.64Å line with a weak Ne V line at 359.37Å, the Fe XIII 359/348 ratio was considered to be the more reliable density diagnostic. The Fe XIII 318/320 ratio was found to be very unreliable due to a significant blending problem of Fe XIII 320.80Å with Ni XVIII 320.55Å. It should be pointed out at this stage that the Fe XIII line observed at ∼359.7Å is in fact a blend of two Fe XIII lines, one at 359.64Å and a weaker one at 359.83Å. For the purposes of this work these blended lines shall be referred to only as the stronger line in the blend, i.e. Fe XIII 359.64Å.

In order to obtain a fast time sequence of images, the windowing capabilities of NIS was used, with a window of 40 wavelength pixels (∼3Å) and 71 spatial pixels (≃119 arc sec). Slit number 5 of CDS was used with a size of 4×240 arc sec^2. The integration time was 10 seconds with a cycle time of ∼13.5 seconds between each set of images. A total of 200 images were obtained in ∼45 minutes. In the end it was decided to rebin the resulting files by a factor of two in time to improve the signal-to-noise at the expense of time resolution. This resulted in 100 images with a time resolution of 27 seconds. For these observations, the solar rotation compensation mode was switched off, and thus the image was generated by the rotation of the Sun.

Standard routines from within the CDS software tree were used in the data reduction, see O'Shea (1997) for details. An automated procedure was used to fit each of the images in the 100 time frames, with the integrated flux used to produce observational line ratios for the particular region of interest along the slit. Individual profiles were selected at random in order to check the accuracy of the automated line fitting.

3.2. SUMER observations

For our density diagnostic study the O IV 1407.39/1401.16 density sensitive line ratio was chosen. Actually, as pointed out in the paper by Wikstol et al. (1997), there are a number of reasons to suggest that density determination using the O IV 1399.7, 1401.2 and 1407.4Å lines may be the only method to infer electron densities in the transition region using SUMER data. In their paper, the above authors pointed out that due to factors such as blending and the weakness of certain lines, there are surprisingly few good line pairs to be found.

The SUMER datasets that were used in this analysis are shown in Table 1 and these will henceforth be referred to only as the last number in the filename shown. The two datasets 165749 and 173109 were observed using slit number 6 of size 0.3 × 120 arc sec^2. For both datasets a window of 50 wavelength pixels (∼2.2Å) and 120 spatial pixels (≃117 arc sec) was used. Each dataset consists of 200 images that were obtained in ∼33 minutes. Again the solar rotation compensation mode was switched off. Each image was taken with an exposure time of 8.95 seconds and a cycle time of 10 seconds. As with the CDS data, it was decided to bin in time by a factor of two to improve the signal-to-noise. Again, standard procedures within the SUMER software tree were used to do the data reduction (see O'Shea, 1997).

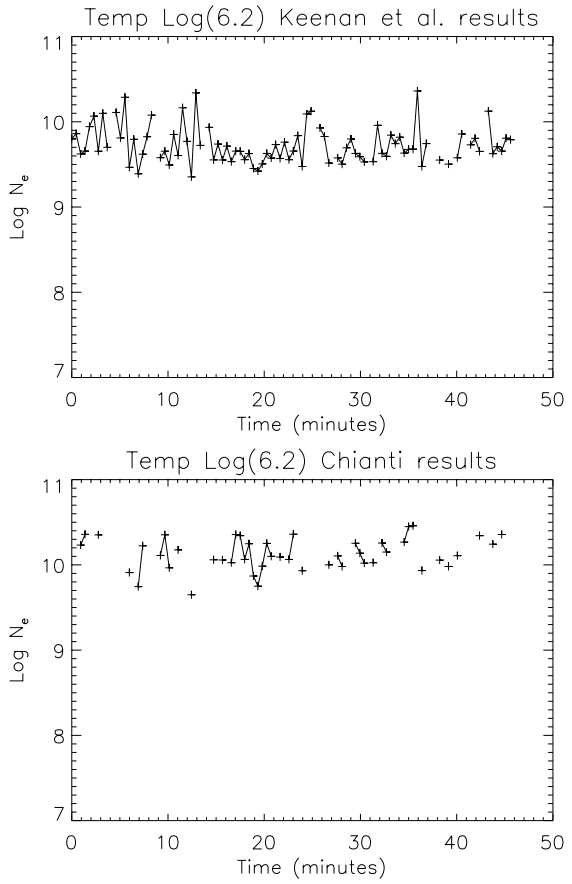

Fig. 2. The derived densities for the 14 to 55 arc sec summed region using the Fe XIII 359/348 ratio. Results are shown for the QUB (Keenan et al.) data and for the CHIANTI database.

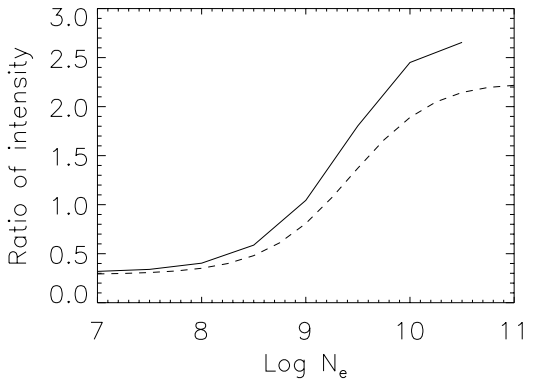

Fig. 3. Theoretical line ratios for Fe XIII 359/348. The QUB (Keenan et al.) results are shown with a continuous line while the CHIANTI data are shown by a dashed line.

4. Results

4.1. Pointing

Before evaluating the different electron density diagnostics, it is important to establish the relative pointings of both instruments. The pointing for the s3477r01 dataset was X=537, Y=–205 while for the 165749 dataset it was X=530, Y=–200 (see Table 1). Thus the solar Y location of the slit for dataset 165749 is 5 arc sec above that for dataset s3477r01. It is necessary however to also take into account the slit sizes of the two instruments. The slit of SUMER is 117 arc sec in length while that of CDS is 119 arc sec. (The spatial pixel size of SUMER is ∼0.97 arc sec while that of CDS is 1.68 arc sec). Thus, it may be seen that position 8 to 49 arc sec in dataset 165749 corresponds in absolute terms along the Y-axis to the region 14 to 55 arc sec in dataset s3477r01. However, the start times for dataset s3477r01 from the CDS data and dataset 165749 from the SUMER data differ by 68 minutes (see Table 1). Taking solar rotation into account there is a distance in X of ∼16 arc sec between the starting locations of each slit.

In dataset s3477r01, a summed region from 14 to 55 was used, while in dataset 165749 the summed region from 8 to 49 arc sec was measured, which correspond to similar Y locations. Results from each of these datasets are shown separately below and the results discussed in Sect. 5.

The start times of datasets s3479r00 and 173109 are separated by 37 minutes, but they observe the same spatial location, taking solar rotation into account. Region 10 to 55 arc sec in dataset s3479r00 and 4 to 49 arc sec in dataset 173109 are therefore observing the same spatial region, within ±1 arc sec.

4.2. s3477r01

In the Fe XIII 359/348 ratio it was found that due to blending of the Fe XIII 359.64Å line with a Ne V line at 359.37Å (Thomas & Neupert 1994, Dere 1978), it was necessary to use two Gaussians in the fit in order to successfully de-blend these lines. The Ne V component in the blend contributed 10–15% of the total flux. The Fe XIII 348.18Å line also suffered blending, in this case with a high temperature line of Fe XVII at 347.406Å. This was again taken into account by fitting two Gaussians to the Fe XIII/Fe XVII line profile.

Because the lines of interest are strong and close together in wavelength we assume that any errors due to line fitting and instrument calibration will be small. In this case errors in the line ratio are estimated to be approximately $\pm 15\%$ or ∼0. 3. This corresponds to errors in the derived density from the Fe XIII ratio of approximately ±0.3 dex.

In Fig. 2, the derived electron densities are shown for the Fe XIII 359/348 ratio in summed region 14 to 55 arc sec. The theoretical line ratios used may be seen in Fig. 3.

The average measured electron density over the observation time in this region, from the QUB results, is Log N_e=9.7 ± 0.2 cm^{-3}. The equivalent value from CHIANTI is Log N_e=10.1 ± 0.2 cm^{-3}.

These compare well with the values of Log N_e=9.7 and 9.5 cm^{-3} found by Keenan et al. (1995) for two active regions on the Sun using the Fe XIII ratios 318.12Å/320.80Å and 256.42Å/251.95Å. It will be noted from the plots that the results derived from CHIANTI give a systematically higher value than those of QUB. Also note that there are gaps in the densities derived from CHIANTI, because a number of the intensity ratios

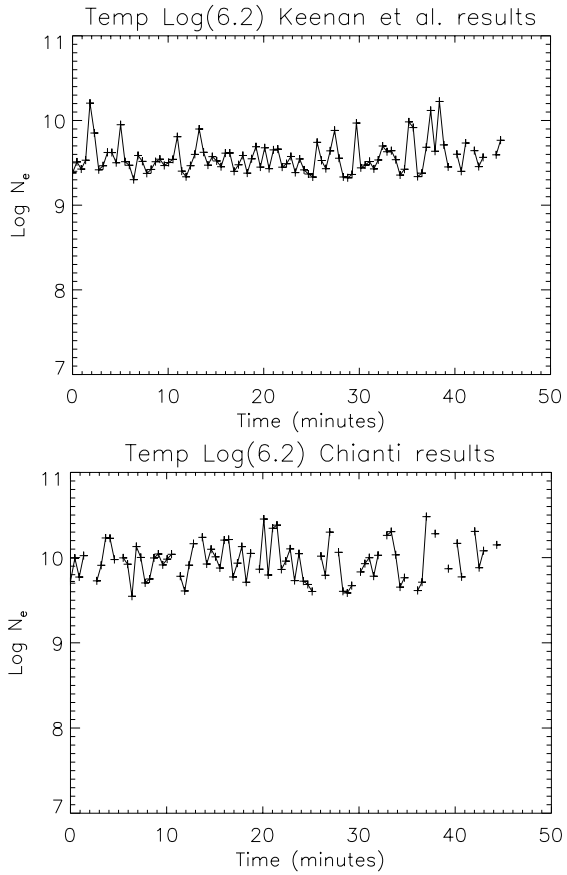

Fig. 4. The derived electron densities for the 10 to 55 arc sec summed region using the Fe XIII 359/348 ratio. Results are shown from the QUB (Keenan et al.) data and from the CHIANTI database.

lie above the high density limit and are therefore not plotted. Only those values plotted have been used to derive an average density.

The average electron density calculated along the whole slit (i.e.∼0–118 arc sec) for the QUB results is Log N_e=9.7 $\pm$ 0.2 cm^{-3}. The equivalent result from CHIANTI is Log N_e=10.1 $\pm$ 0.2 cm^{-3}. Assuming the ionization equilibrium temperature of Fe XIII to be Log T_e=6.2 K (Arnaud & Rothenflug 1985), this implies coronal electron pressures of 15.9 cm^{-3} K and 16.3 cm^{-3} K, respectively.

4.3. s3479r00

In Fig. 4, results are shown for the region 10 to 55 arc sec. The average electron density for this region over the observation time is Log N_e=9.6 $\pm$ 0.2 cm^{-3} from the QUB results, and Log N_e=10.0 $\pm$ 0.2 cm^{-3} from CHIANTI.

The average electron density over the whole slit (∼0–118 arcsec) has a value of Log N_e=9.5 $\pm$ 0.1 cm^{-3}, using the QUB results. The corresponding average value found from CHIANTI is Log N_e=10.0 $\pm$ 0.2 cm^{-3}. These imply coronal electron pressures of 15.7 cm^{-3} K and 16.2 cm^{-3} K respectively. Thus there is no long term variation in the coronal electron density in this region over a period from 16:57 UT to 18:04 UT, i.e. a spatial region covering ∼12 arc sec in the East-West direction.

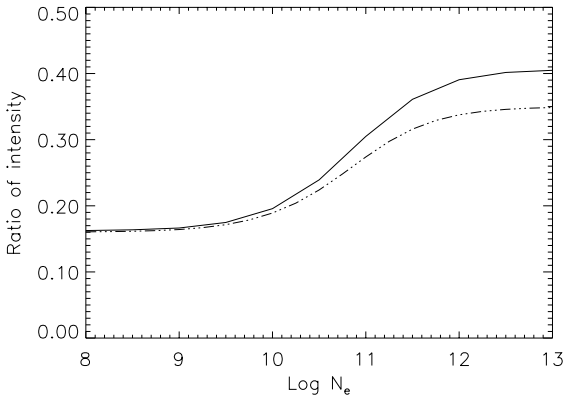

Fig. 5. Theoretical line ratios for O IV 1407/1401. The QUB results are shown as a continuous line, while the CHIANTI data are shown by the dot-dashed line.

4.4. 165749

For this dataset we choose to observe the region from 8-49 arc sec. This corresponds to the whole of a bright region at the bottom of the slit. The theoretical O IV curves used to derive Log N_e are shown in Fig. 5 while the resulting values are shown in Fig. 6. The difference between the CHIANTI and QUB O IV theoretical line ratios apparent at higher electron densities, is due to the different A-values used by these groups.

Errors in the line ratio are estimated to be approximately $\pm 10\%$ or ∼0.03. This corresponds to errors, in the derived density from the O IV ratio, of approximately $\pm$0.25 dex.

The electron density, based on the QUB atomic data begins at a maximum value (in this case Log N_e=11.3 cm^{-3}) and then settles down to be roughly at Log N_e=10.8 cm^{-3}. The average value over the full observation time is Log N_e=10.8 $\pm$ 0.2 cm^{-3}. The equivalent average electron density from CHIANTI is Log N_e=11.0 $\pm$ 0.3 cm^{-3}. Small surges in density are present at 15 and 18 minutes, these will be discussed further in another paper (Doyle et al. 1998). They are more apparent in the results from CHIANTI for which an electron density of Log N_e=11.8 cm^{-3} may be assigned to the peak at 15 minutes.

Along the whole slit (i.e. summing over the full ∼117 arc sec) the average electron density was found to be Log N_e=10.5 $\pm$ 0.3 cm^{-3} using the QUB results. The equivalent value from CHIANTI was Log N_e=10.7 $\pm$ 0.2 cm^{-3}. These imply transition region electron pressures of 15.7 cm^{-3} K and 15.9 cm^{-3} K respectively, if we assume that the O IV line has a temperature of maximum abundance at Log T_e=5.2 (Arnaud and Rothenflug, 1985).

4.5. 173109

The region 4 to 49 arc sec comprises a bright region at the bottom of the slit. The derived electron densities for this region are shown in Fig. 7. A clear upsurge in density is visible here

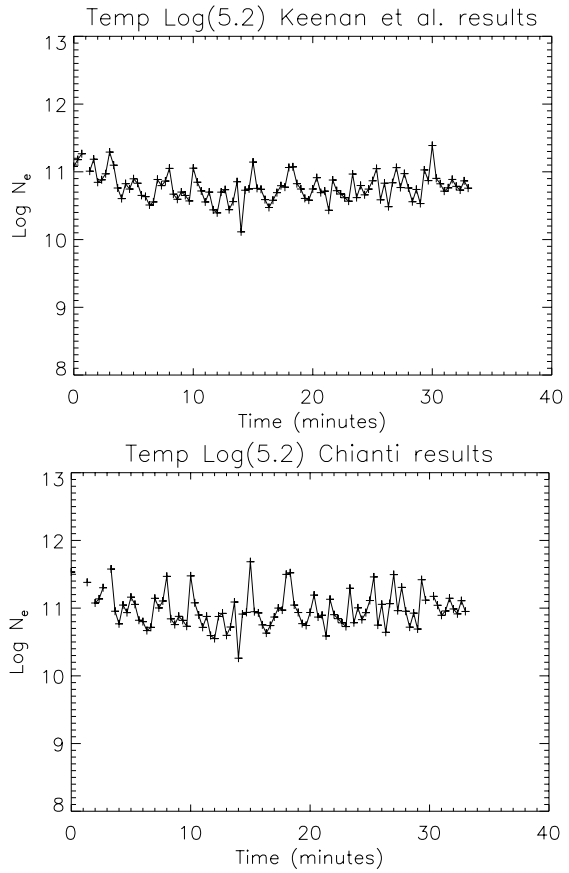

Fig. 6. The derived densities for the O IV 1407/1401 ratio, for the summed region 8 to 49 arc sec in dataset 165749. Results are shown from the QUB (Keenan et al.) data and from the CHIANTI database.

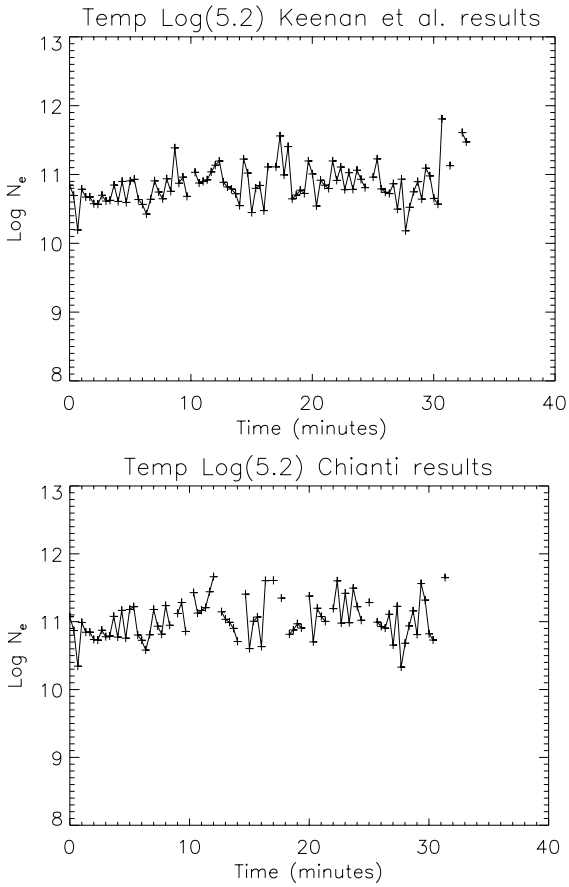

Fig. 7. The derived densities for the O IV 1407/1401 ratio, for the summed region 4 to 49 arc sec in dataset 173109. Results are shown from the QUB (Keenan et al.) data and from the CHIANTI database.

in the QUB results towards the end of the observation with Log N_e reaching 11.8 cm^{-3} . It is clear that there is a considerable increase in electron density in a relatively short time which may indicate that a small scale flaring event is occurring.

The average value over the observation time is Log N_e=10.9 $\pm$ 0.3 cm^{-3}, from the QUB results while the CHIANTI results imply Log N_e=11.0 $\pm$ 0.3 cm^{-3}.

Along the whole slit (i.e. summing over the full $\sim$117 arc sec) the average electron density was found to be Log N_e=10.8$\pm$ 0.4 cm^{-3} using the QUB results. The equivalent value from CHIANTI is Log N_e=11.0 $\pm$ 0.5 cm^{-3}. These densities imply electron pressures of 16.0 cm^{-3} K and 16.2 cm^{-3} K respectively in the transition region.

Table 2. A summary of the various electron densities and pressures obtained from the different datasets using the QUB diagnostics. The results from CHIANTI are shown in brackets.

Dataset	Region (Arc sec)		Log N_e (cm^{-3})	Log P_e (cm^{-3} K)
165749	8-49	TR	10.8(11.0)	16.0(16.2)
165749	Whole slit	TR	10.5(10.7)	15.7(15.9)
s3477r01	14-55	Corona	9.7(10.1)	15.9(16.3)
s3477r01	Whole slit	Corona	9.7(10.1)	15.9(16.3)
173109	4-49	TR	10.9(11.0)	16.1(16.2)
173109	Whole slit	TR	10.8(11.0)	16.0(16.2)
s3479r00	10-55	Corona	9.6(10.0)	15.8(16.2)
s3479r00	Whole slit	Corona	9.5(10.0)	15.7(16.2)

5. Discussion and conclusions

What do the results in Sect. 4 tell us about the transition region? Firstly we will do a comparison of the s3477r01 and 165749 datasets using just the QUB results. As discussed above, both these datasets observe a region some 16 arc sec apart in X. In dataset s3477r01 the region 14 to 55 arc sec was measured using the Fe XIII 359/348 ratio and found to have an average electron density over the observation time of Log N_e=9.7 cm^{-3}. This implies a coronal electron pressure of 15.9 cm^{-3} K. The corresponding region 8 to 49 arc sec measured in the transition region by dataset 165749 was found to have an electron density of Log N_e=10.8 cm^{-3}, corresponding to a transition region electron pressure of Log 16.0 cm^{-3} K. These results clearly offer little evidence of a constant electron density from the transition region to the corona, despite the fact that we are not even observing the same spatial region. Instead, they offer strong evidence for a constant electron pressure, i.e. the measured electron pressures from both diagnostics differ by only 0.1 dex.

Similar conclusions are obtained by using the CHIANTI results. For the Fe XIII 359/348 ratio, the results for the s3477r01 dataset imply an electron density of Log N_e=10.1 cm^{-3} and a corresponding coronal electron pressure of 16.3 cm^{-3} K. For the O IV 1407/1401 ratio the results for the 165749 dataset are Log N_e=11.0 cm^{-3}, giving a transition region electron pressure of Log 16.2 cm^{-3} K. Again we see that the difference in pressures is only 0.1 dex, indicating a constant electron pressure from the transition region to the corona.

Similarly it is possible to do a comparison between datasets s3479r00 and 173109. As discussed previously region 10 to 55 arc sec in dataset s3479r00 and 4 to 49 arc sec in dataset 173109 observe the same spatial region. Region 10 to 55 arc sec was measured in dataset s3479r00 and found to have an average electron density over the observation time of Log N_e=9.6 cm^{-3} using the QUB results and Log N_e=10.0 cm^{-3} using CHIANTI. These correspond to coronal electron pressures of Log 15.8 cm^{-3} K and Log 16.2 cm^{-3} K respectively. The average electron density over the observation time in region 4 to 49 arc sec of dataset 173109 was found to be Log N_e=10.9 cm^{-3} using the Keenan et al. results and Log N_e= 11.0 cm^{-3} using CHIANTI. These correspond to pressures of Log 16.1 cm^{-3} K and Log 16.2 cm^{-3} K respectively in the transition region.

From all these results it is clear that there is little evidence of a constant electron density between the transition region and corona and we must therefore conclude that a constant electron pressure is a more likely explanation. This appears at first to contradict the findings of Feldman & Laming (1993). For the present data we used a coronal line at a temperature of Log T_e=6.2 K comparing it to a transition region line at Log T_e=5.2 K. It may be that the burst model proposed by Feldman & Laming is relevant for events such as the transition region explosive events (Dere 1994) which are thought to be caused by reconnection of magnetic field lines in a process similar to that thought to be responsible for nanoflares. These occur in a narrow temperature band comprising only transition region plasma. In-fact, the lines used by Feldman & Laming covered only transition region plasma and were for active region plasma conditions.

A constant electron pressure between the transition region and conora would suggest that the transition region is simply a time varying interface between the chromosphere and corona and is not formed in unresolved fine structures that are magnetically and thermally disconnected from the corona.

Acknowledgements. Research at Armagh Observatory is grant-aided by the Dept. of Education for N. Ireland while partial support for software and hardware is provided by the STARLINK Project which is funded by the UK PPARC. This work was supported by PPARC (grant GR/K43315) and by the Leverhulme Trust. We would like to thank the SUMER, CDS and EIT teams at Goddard Space Flight Center for their help in obtaining the present data. The SUMER project is financially supported by DLR, CNES, NASA, and the PRODEX programme (Swiss contribution). SUMER is part of SOHO, the Solar and Heliospheric Observatory of ESA and NASA.

References

Arnaud, M. & Rothenflug, R., 1985, A&AS, 60, 425
Brage, T., Judge, P.G. & Brekke, P., 1996, ApJ, 464, 1030
Cook, J.W., Keenan, F.P., Dufton, P.L. et al., 1995, ApJ, 444, 936
Dere, K.P., 1978, ApJ, 221, 1062
Dere, K.P., Mason, H.E., Widing, K.G. & Bhatia, A.K., 1979, ApJS, 40, 341
Dere, K.P., 1982, Sol Phy, 77, 77
Dere, K.P., 1994, Adv. Space Res., 14, 13
Dere, K.P., Landi, E., Mason, H.E., Monsignori-Fossi, B.C. & Young, P.R., 1997, A&A Supl. Series, 125, 149
Doschek, G.A., 1984, ApJ, 279, 446
Doyle, J.G., Perez, M.E. & O'Shea, E. 1998, A&A (to be submitted)
Dufton, P.L., 1977, Comp. Phys. Comm., 13, 25
Dwivedi, B.N. & Gupta, A.K., 1992, Sol Phy, 138, 283
Dwivedi, B.N. & Gupta, A.K., 1994, Sol Phy, 155, 63
Feldman, U., 1992, ApJ, 385, 758
Feldman, U., Laming, J.M., Mandelbaum, P., Goldstein, W.H. & Osterheld, A., 1992, ApJ, 398, 692
Feldman, U. & Laming, J.M., 1993, ApJ, 404, 799
Flower, D.R. & Nussbaumer, H., 1974, A&A, 31, 353
Flower, D.R. & Pineau des Forets, G., 1973, A&A, 24, 181
Flower, D.R. & Nussbaumer, H., 1975, A&A 45, 145
Harrison, R.A., Sawyer, E.C., Carter, M.K. et al., 1995, Sol Phy 162, 233
Keenan, F.P., Foster, V.J., Drake, J.J., Tayal, S.S. & Widing, K.G., 1995, ApJ, 453, 906
Laming, J.M. & Feldman, U., 1992, ApJ, 386, 364
Nussbaumer, H. & Storey, P.J.: 1982, A&A, 115, 205
O'Shea, E., Foster, V.J., Keenan, F.P., Doyle, J.G., Reid, R.H.G., Zhang, H.L. & Pradhan, A.K., 1996, A&A, 306, 621
O'Shea, E., 1997, PhD thesis (Queens University Belfast)
Tayal, S.S., 1995, ApJ, 446, 895
Thomas, R.J., & Neupert, W.M., 1994, ApJS, 91, 461
Vernazza, J.E. & Mason, H.E., 1978, ApJ, 226, 720
Wikstol, O., Judge, P.G. & Hansteen, V.H., 1997, ApJ, 483, 972
Wilhelm, K., Curdt, W., Marsch, E. et al., 1995, Sol Phy, 162, 189
Wilhelm, K., Lemaire, P., Curdt, W. et al., 1997, Sol Phy, 170, 75
Zhang, H.L., Graziani, M. & Pradhan, A.K., 1994, A&A, 283, 319